PHYSICAL REVIEW D VOLUME 16, NUMBER 7 1 OCTOBER 1977

Simultaneous measurement of the spin parameters P and C_{NN} in pp elastic scattering at 2, 3, 4, and 6 GeV/c†

D. Miller and C. Wilson
Northwestern University, Evanston, Illinois 60201

R. Giese, D. Hill, K. Nield, P. Rynes, B. Sandler, and A. Yokosawa
Argonne National Laboratory, Argonne, Illinois 60439

(Received 1 March 1977)

Using the polarized-beam facility at Argonne National Laboratory and a polarized proton target, simultaneous measurements of the spin parameter P and the spin correlation term C_{NN} were made. Data were obtained and analyzed at beam momenta of 2, 3, 4, and 6 GeV/c in the momentum-transfer-squared interval $0.1 \leq |t| \leq 2.8$ (GeV/c)^2. A preliminary phase-shift analysis of the 2- and 3-GeV/c data is discussed and a comparison with predictions of a particular Regge-pole model at all four energies is made.

I. INTRODUCTION

Until the last few years, there was little excitement connected with simple p-p elastic scattering. Precise total- and differential-cross-section measurements had been performed, showing relatively smooth s and t dependences.[1] Results of polarization experiments, in particular P and C_{NN}, were larger than many expected but did not show, within their errors, much structure. However, with the unexpected results of rising total cross section from CERN and Fermilab, change of slope in $d\sigma/dt$ at $t \simeq -0.12$ (GeV/c)^2, and the emergence of a dip at $t \simeq -1.5$ (GeV/c)^2 at high energies[2,3], interest was renewed in p-p scattering. In addition, polarization experiments using improved polarized targets showed very definite structure at large t [$0.6 \leq |t| \leq 6$ (GeV/c)^2].[4-6]

At the same time the Zero Gradient Synchroton (ZGS) at Argonne National Laboratory (ANL) was developing the capability to accelerate polarized protons to high energies.[7] Using this facility, and an already available polarized proton target, we were able to simultaneously measure the spin parameters P and C_{NN} in the beam momentum range of 2 to 6 GeV/c. A preliminary report of a subsample of these data has been previously reported,[8] and the results are seen not to have significantly changed except for a reduction in the error bars.

This momentum interval is of interest because it connects the two energy ranges that have been reasonably well described by very different approaches. Data at 2 GeV/c and below have been described with some success by phase-shift analyses,[9,10] while 6 GeV/c and above have been fitted reasonably well by various Regge[11] and optical models.[12-14] Extrapolations of these high-energy fits, however, to lower energies have not been particularly successful. So while the P and C_{NN} measurements by themselves are insufficient to determine any of the five complex amplitudes (see Appendix), they will impose strong constraints on the energy and angular predictions of any model.

A description of the experimental apparatus will first be presented, followed by a discussion of the data analysis and then a comparison of these results with current model predictions.

II. EXPERIMENTAL EQUIPMENT

A. Polarized target

The polarized proton target (PPT) used in this experiment was PPT III designed and built at ANL. This target is of the N-type design, that is, the direction of polarization is normal to the nominal plane of scattering. In this case the spin axis is vertical and scattering is in the horizontal plane. Because of the finite size of the scattering aperture, one can, in principle, detect events with the normal to the plane of scattering at an angle as large as $\pm 30°$ to the vertical.

The magnet used with this target consisted of two pair of superconducting Helmholtz coils. This arrangement provided a field of 2.5 T with a cylindrical volume, 2 cm high and a radius of 5 cm, of uniform field ($\Delta B/B < 0.0007$). The temperature was maintained at 4.2 K by means of a ^{4}He refrigeration system.

The target material used was ethylene glycol ($HOCH_2CH_2OH$) doped with $K_2Cr_2O_7$ and maintained at 0.4 K by means of a ^{3}He refrigerator. The polarization was dynamically produced by supplying microwave energy to cause an energy level transition to take place between the free protons and the charged Cr radical in the target material. For a detailed discussion of the polarizing process, see Refs. 15–17.

The value of the nuclear polarization was monitored by taking nuclear magnetic resonance (NMR) signals,[18] N_n, approximately every 15 sec. These signals are a direct measure of polarization, P_n, of the free hydrogen in the target. These signals can then be compared to equivalent signals taken during thermal equilibrium, N_{TE}, conditions (i.e., no microwave) where polarization, P_{TE}, is easily calculated from simple Boltzmann formulas. Using P_{TE} as a calibration point, P_N can be simply determined. The N_{TE} signal represents the largest systematic error for polarization with an error of $\Delta N_{TE}/N_{TE} < 0.03$.

To reduce errors due to slow changes in beam quality and chamber efficiency the polarization was reversed every 3–4 hr to average over such changes. The changeover time from beginning to 50% reversed polarization was 10–20 min. Average polarizations of 70–80% were achieved per spin direction.

The NMR signals were analyzed by a PDP-11 computer and were stored on Dec tape. In addition, the magnetic field and microwave frequency were continuously monitored and automatically corrected when necessary if they started to drift. Polarizations were calculated on-line using an approximate N_{TE} value and the results stored with the scattering data each spill. The final polarization was obtained by later analysis of the N_{TE} signals.

B. Polarized beam

Beam polarization, during our running period, was 65–70% with the spin direction alternating between up and down every spill. The polarization was monitored on a pulse-by-pulse basis with averages made every 15 min. Two separate polarimeters were used at different stages of the acceleration cycle. One was positioned at the end of the 50-MeV Linac, prior to injection to the main ring, and the other immediately after extraction from the ZGS.

Intensities on target varied from 40 000/pulse at 2 GeV/c to 400 000/pulse at 6 GeV/c at a rate of about 24 pulses/min. Differences in rate were simply the result of extraction and transport efficiencies of the ZGS and the beam transport magnets. For detailed descriptions of the polarized ion source and acceleration procedures see Refs. 19–24.

C. Detection equipment and event logic

The detection equipment consisted of scintillation counters, which provided a fast trigger, and an array of multiwire proportional chambers (MWPC's) which defined the trajectories of the incident and scattered particles. The counters and chambers are shown schematically in Fig. 1.

The beam line was tuned for each momentum by first centering the beam on the *MH* counter array. This array consisted of eight scintillation counters spaced horizontally across the beam line. Next the MWPC beam chambers (BC) were used to detect beam particles and calculate, on-line, the phase space of the beam. We then made fine adjustments to the beam magnets to optimize the beam size and divergence at the target position.

The counters S_0, S_1, and S_2 defined the presence of a beam particle. The counter AB, which had a $1\frac{1}{4}$-in. hole, vetoed particles which were too far off the beam axis to strike the target. Thus the coincidence $B = S_0 \cdot S_1 \cdot S_2 \cdot \overline{AB}$ was defined to be a good beam trigger and was used to normalize the final elastic-event rates.

A candidate for an elastic event was then determined by the coincidence of B with at least one R and one L counter. This logic thus required that a beam particle struck the target and at least two

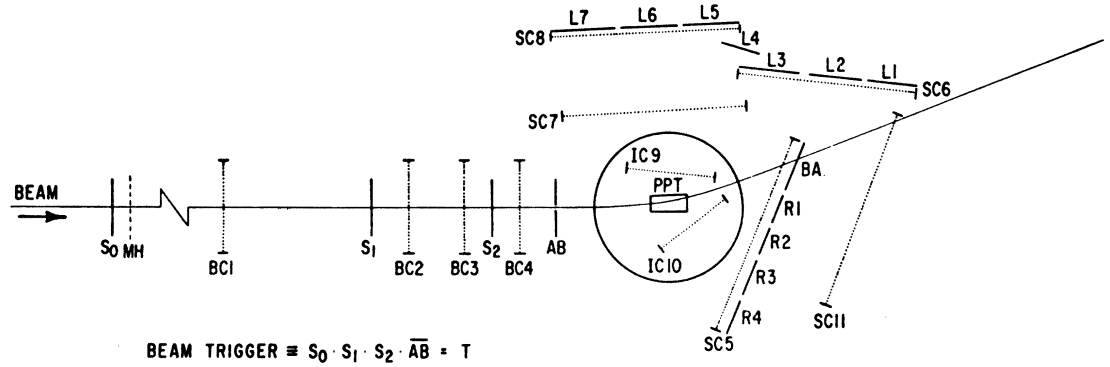

FIG. 1. Layout of experimental equipment (not drawn to scale).

charged particles emerged. To reduce the data rate due to inelastic events, counters were installed to veto events with additional particles present.

Counters BA and $L1$ were put into veto to eliminate inelastic events with a fast forward particle. Counters ($A1, A2, A3, A4$), not shown in Fig. 1, were placed as close as possible to the target, above and below the scattering plane, to further reduce the background. These counters consisted of three layers of plastic scintillator (total thickness 300 mil) and two layers of tantalum (180 mil or 1.2 radiation lengths) which was used to convert photons.

This then defined the fast trigger for a potentially good elastic event. Before the data were recorded on magnetic tape, the L, R, and MH counters were held in Lecroy (LRS 902) Omnilogic modules and a simple logic test was made for correlations among L and R counters. This test consisted of requiring a reasonable L-R correlation, based on elastic kinematics. It did not rule out, however, the presence of multiple L and R counter hits since some counters overlapped. Additional checks of L and R counters were later made off-line. When the fast logic indicated that a potential elastic event was present, the wire information was held until read in by the on-line computer (ASI 6050). There were three basic types of MWPC's used. All chambers were composed of a pair of wire planes, X and Y, with 2-mm wire spacing, aluminized Mylar high-voltage planes and used an Ar-CO_2 (65-35%) gas mixture. The beam chambers (BC) had 64 wires in both the X and Y planes and the scattering chambers (SC) had 256 vertical wires and 128 horizontal. Both types of chambers were used outside the magnetic field and had the electronics attached directly to the wire planes.

The inner chambers (IC) had 24 horizontal and 128 vertical wires and were designed to be placed next to the target inside the magnetic field. The wire signals were led out via twisted pair ribbon cables. The cables were shielded by a wire mesh to reduce noise pickup, and a differential amplifier (MECL 1020, gain ≈ 6) was spliced into the signal lines near the chamber to compensate for signal attenuation.

The data stored on tape included, in addition to the wire hits, the event number, beam polarity, which L, R, and MH counters were on and, after each spill, the contents of all on-line scalars and the current target polarization.

For use as an on-line monitor, the data were continuously sampled, wire maps of each MWPC were displayed, and correlation histograms of the R and L counters were made. In addition, the on-line scalars and beam-magnet power supplies were monitored and any sudden change in scalar ratios or magnet settings produced a warning message to the operator.

III. DATA ANALYSIS

The quantities that we wish to extract from our data are the differential cross sections of elastic scattering in states of pure initial spin normal to the scattering plane. Such a cross section can be expressed in terms of the initial proton spins as

$$\sigma(P_B, P_T, t) = \sigma_0(t)[1 + (P_B + P_T)P(t) + P_B P_T C_{NN}(t)],$$

where P_B and P_T are the values of the beam and target polarization, t is the square of the four-momentum transfer, and σ_0 is the unpolarized differential cross section. The axis of polarization is then defined to be

$$\hat{n} = \vec{P}_{in} \times \vec{P}_{fin} / |\vec{P}_{in} \times \vec{P}_{fin}|,$$

where $\vec{P}_{in}$ is the incident beam momentum and $\vec{P}_{fin}$ is the momentum of the particle scattered to beam right. Since P and C_{NN} are the parameters of interest here, the acceptance of our apparatus is not directly included in the calculation of $\sigma(P_B, P_T, t)$. Therefore, the quantity σ_0 we calculate is actually the product of the real cross section and our acceptance, but P and C_{NN} are free of this acceptance factor.

The analysis of an event consists of first examining the wire pattern in each chamber, grouping sets of adjacent wires and converting these positions to coordinates in real space, then calculating the relevant kinematics and separating elastic events from background. Because of the sheer volume of data (about 17 000 000 raw events), considerable filtering was necessary to eliminate obvious inelastics. Both filtering and final analysis were done on the IBM 370/195 at ANL.

For an event to be saved for final analysis, it has to meet certain rather simple criteria. The first concerns the left and right trigger counters. Events with multiple left and right hits, except for overlapping counters, are rejected as well as left-right correlations that are obviously inelastic.

Because of the relatively long memory time of the chambers (~50 ns) compared to the scintillation counters (5–10 ns), there were a significant number of events (5–10%) with extra wires on not associated with the event which triggered the fast logic. Some of these wires can be eliminated under certain conditions. If the wires are definitely in the beam region of chambers 5 or 11, they are considered to be beam memory and thus eliminated. In addition, if a wire is on that is not covered by an R or L counter that is also on, it is

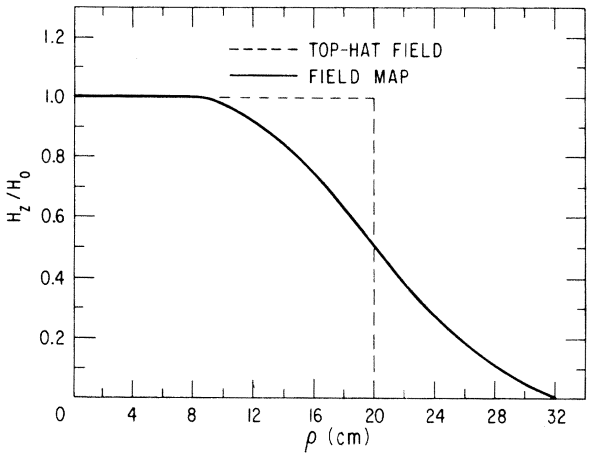

FIG. 2. Vertical component of the magnet field as a function of radial distance from axis in the central plane.

assumed to be memory and eliminated.

Once these wire cuts are made, a check is performed to see if there is just one track to beam right and one to beam left. When a group appears in more than one chamber, it is required that they be in an overlap region of the chambers.

Finally, the beam chambers are used to calculate a beam trajectory. If one, and only one, straight line can be fitted through these chambers, a beam slope and intercept at the projected center of the target is calculated. If the event passes these tests, the beam trajectory and the filtered wire information is output to tape. The fraction of events that pass the filter is about 70% at 2 GeV/c and 50% at 6 GeV/c.

The major problem in analyzing the trajectories of the beam, scattered, and recoil particles is the magnetic field of the target magnet. Since there were insufficient chambers, even in principle, to accurately reconstruct the trajectories at the vertex, certain simplifying assumptions had to be made in the field corrections.

The magnetic-field corrections consist of taking the hit in a given chamber plane and shifting it by a correction term to where the hit would have been if the scattered particle had not gone through any magnetic field. The assumptions used here are that the particle is from an elastic event and that scattering takes place in the horizontal plane. The first assumption is needed to give a definite relation between scattering angle and momentum. The second assumption, because the ϕ region (the angle between the scattering normal, $\hat{n}$, and the vertical axis) of the data sample used is small ($|\phi| \leq 10°$), introduces only a small error ($\leq 2\%$) in the correction term. One other simplifying assumption was that the magnetic field was a "top-hat" field. This approximation is compared with the correct field map in Fig. 2. This assumption, for the forward particle, also introduces a small error ($\leq 3\%$) in the correction term.

Adding all these systematic errors together introduces a total error of less than 4% to the calculated value of t for all t and beam momenta.

Using the field-corrected track positions in the scattering chambers one can, with the inner chambers, reconstruct the vertex point to within ± 0.5 cm and then proceed to calculate all the relevant scattering kinematics.

The quantities calculated are the polar angle, θ and ϕ (see Fig. 3), for both scattered (θ_s, ϕ_s, beam right) and recoil particles (θ_r, ϕ_r, beam left) relative to the beam at the vertex. At this point a data summary tape is generated which contains for each event the θ and ϕ angles for both scattered and recoil particles, the beam trajectory, L, R, and MH counter bit patterns, and information telling which chambers were used in the event reconstruction.

The two kinds of background present are inelastics and quasielastic scattering off of bound protons in the other, more complex nuclei present in the target. Quasielastic events[25,26] are the major source of background error since they are, in a sense, elastic events with a Fermi-momentum distribution added to the initial target proton. The effect of this is to randomly smear out the angular and momentum correlations one would expect from true elastic events. Inelastics are then considered to be anything else from either free protons or other nuclei but are suppressed by the requirement of two and only two scattered particles.

Elastic events have two distinctive characteristics which, in general, distinguish them from background. The first is that the beam, scattered,

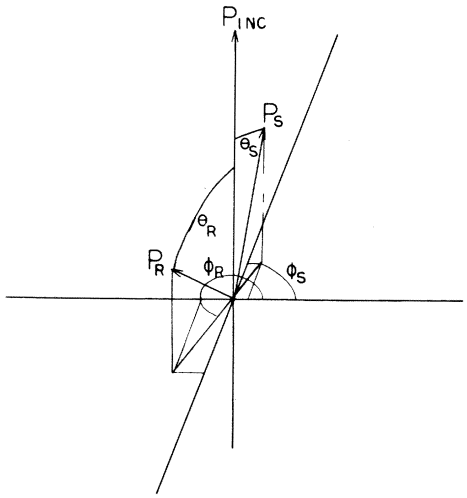

FIG. 3. Vector diagram defining kinematic variables.

and recoil particles must be coplanar, or

$$\Delta\phi \equiv \phi_s - \phi_r + 180° = 0 .$$

The other property is the correlation between θ_s and θ_r,

$$(\tan\theta_s)(\tan\theta_r) = 4M^2/W^2 ,$$

where M is the proton mass and W is the total center-of-mass energy. However, due to resolution uncertainties and multiple scattering in the target and cryostat walls, these kinematic constraints must be relaxed.

Since the multiple scattering of recoil and scattered particles will smear out the observed angular correlations for free events in a qualitatively similar way as a quasielastic scatter, we must determine if we can distinguish between them.

The momentum distribution of a proton in carbon can be roughly approximated by a Gaussian with a standard deviation of about 125 MeV/c.[25,26] One would then expect that if one chose a particular scattering angle for the forward particle the recoil angular distribution would, crudely speaking, be Gaussian distributed around the elastic angle with a standard deviation of about $125/P_r$, where P_r is the recoil momentum (in MeV/c) expected if this were an elastic event.

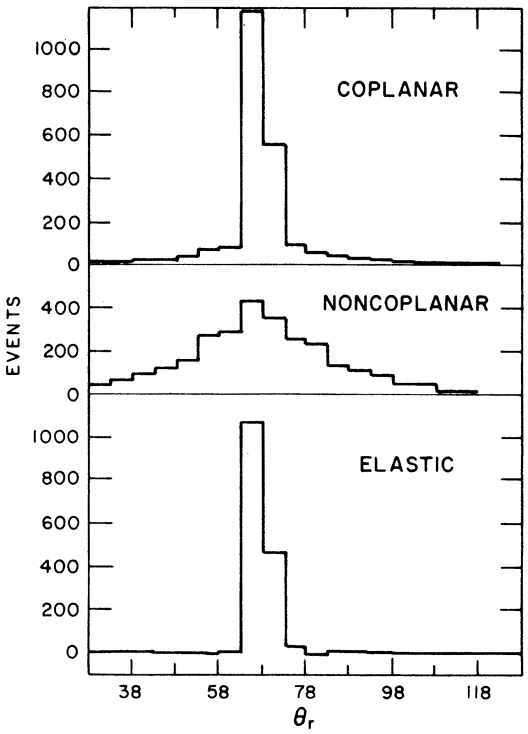

FIG. 5. The elastic-event signal obtained by subtracting noncoplanar events from coplanar events.

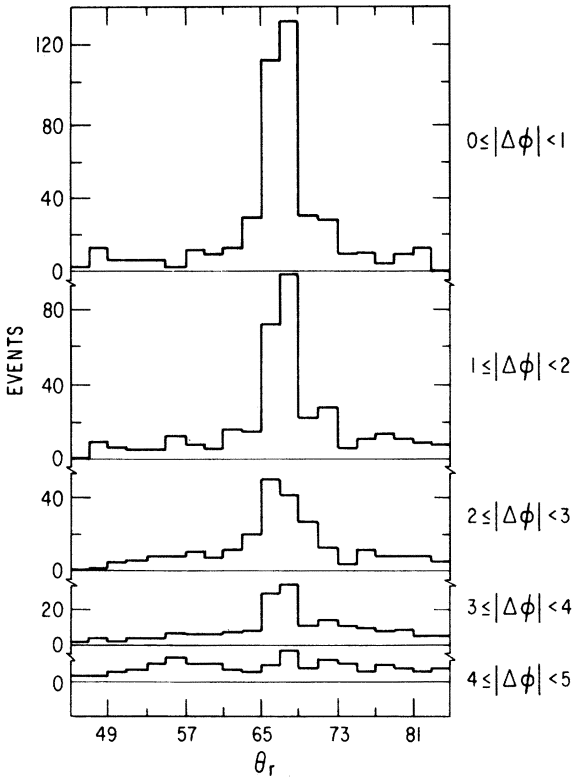

FIG. 4. θ_r distributions for various slices in $|\Delta\phi|$.

The lowest $|t|$ value we go to is approximately $|t| = 0.12$ (GeV/c)^2 with a $P_r = 350$ MeV/c. If the recoil particle were to go through the entire width of the target (2 cm or 1.66 g/cm^2) and the cryostat walls (1.2 g/cm^2) and we were to use the scattering length for carbon (44.6 g/cm^2) we would have[27]

$$(\langle\theta^2\rangle_{MS})^{1/2} = \frac{21}{P_r\beta_r}\left(\frac{X}{X_0}\right)^{1/2} = \frac{21}{122}\left(\frac{2.86}{44.6}\right)^{1/2} = 42 \text{ mrad} = 2.4° .$$

The scattering angle for quasielastic scattering is

$$(\langle\theta^2\rangle_Q)^{1/2} = \frac{125}{350} = 360 \text{ mrad} \approx 20° .$$

Therefore $(\langle\theta^2\rangle_Q)^{1/2}/(\langle\theta^2\rangle_{MS})^{1/2} \approx 8$, which means that the elastic signal should appear as a narrow spike on top of a much broader quasielastic bump.

For most of the events in this experiment the scattered, forward, particle has a small ($\lesssim 0.25°$ at 2 GeV/c) multiple-scattering error and resolution uncertainty of $\approx 0.2°$. The slow recoil particle has a resolution error also of about 0.2° but has a very large multiple-scattering error due to its low momentum ($P_r = 0.3$–1.0 GeV/c). Because of its much smaller errors, all the elastic kinematics will be defined by the scattered particle. These

include the momentum transfer, t, and the normal to the scattering plane, $\hat{n}$. The data are then binned into equal intervals of θ_s (1° bins for 2, 3, and 4 GeV/c and 0.5° for 6 GeV/c). The data are then further divided into intervals of $|\phi_s|$. This is done since the beam and target polarizations were both vertical but $\hat{n}$ is at an angle of ϕ_s to this direction. This introduces small (< 2%) differences in effective polarization. Next, for each of the θ_s and ϕ_s bins, plots of θ_r vs $|\Delta\phi|$ are made.

Figure 4 is an example of one such set of plots. These particular plots are of 2-GeV/c data with both beam and target polarization positive and with $20.5° \leq \theta_s \leq 21.5°$ [$\bar{t} \approx -0.47$ (GeV/c)^2] and $|\phi_s| \leq 5°$. Each plot is a θ_r distribution for different slices of $|\Delta\phi|$. In this t interval θ_r, according to elastic kinematics, covers a 1.5° range which, when coupled with a multiple scattering error of 0.8°, is consistent with the observed peak. In doing the background subtraction, the data for $|\Delta\phi| \leq 3°$ are summed and defined to be "coplanar" and the interval $4° \leq |\Delta\phi| \leq 8°$ is defined as noncoplanar as shown in Fig. 5. Because no significant differences in shape of the background distributions are found among the four spin combinations, the noncoplanar plot is the sum of the four spin states. The dis-

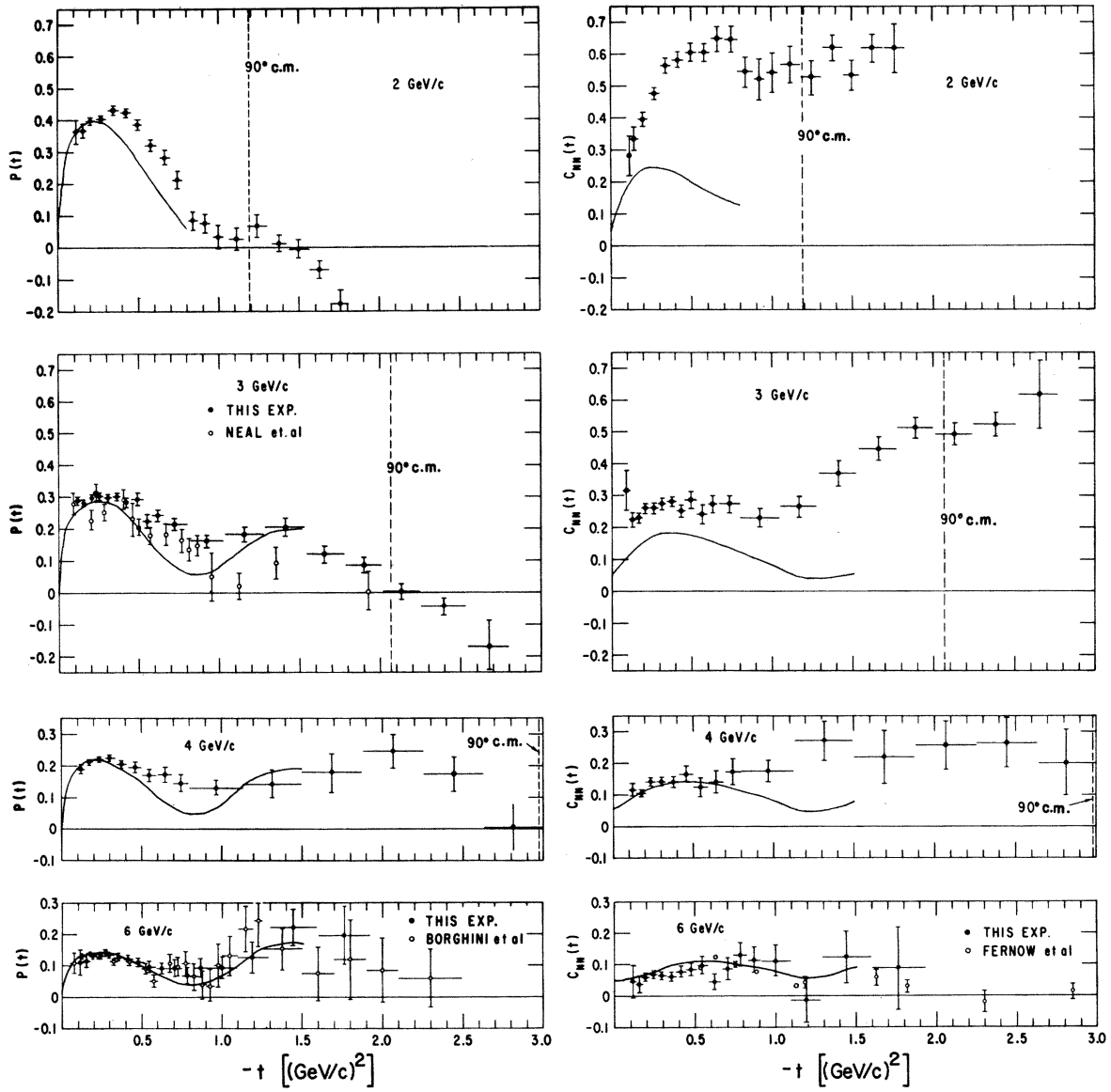

FIG. 6. P and C_{NN} plotted as functions of t at 2, 3, 4, and 6 GeV/c. The smooth curves are predictions from Ref. 11. Existing data are compared at 3 and 6 GeV/c (Refs. 29–31).

TABLE I. P and C_{NN} for various incident momenta and t.

$\bar{t}$ [(GeV/c)^2]	t_{min} [(GeV/c)^2]	t_{max} [(GeV/c)^2]	P	C_{NN}
		2 GeV/c		
0.118	0.107	0.130	0.362 ± 0.037	0.287 ± 0.061
0.155	0.130	0.182	0.365 ± 0.021	0.336 ± 0.036
0.210	0.182	0.241	0.397 ± 0.012	0.396 ± 0.021
0.272	0.241	0.306	0.402 ± 0.012	0.482 ± 0.019
0.341	0.306	0.377	0.429 ± 0.015	0.564 ± 0.025
0.414	0.377	0.453	0.424 ± 0.014	0.583 ± 0.024
0.492	0.453	0.533	0.387 ± 0.016	0.603 ± 0.027
0.574	0.533	0.616	0.318 ± 0.017	0.601 ± 0.028
0.659	0.616	0.702	0.280 ± 0.024	0.646 ± 0.040
0.745	0.702	0.789	0.210 ± 0.026	0.642 ± 0.042
0.833	0.789	0.877	0.085 ± 0.029	0.546 ± 0.048
0.922	0.877	0.966	0.077 ± 0.029	0.524 ± 0.064
1.010	0.966	1.054	0.031 ± 0.037	0.539 ± 0.062
1.120	1.054	1.185	0.026 ± 0.035	0.562 ± 0.057
1.249	1.185	1.312	0.066 ± 0.035	0.524 ± 0.054
1.379	1.312	1.435	0.012 ± 0.025	0.616 ± 0.041
1.494	1.435	1.552	−0.005 ± 0.029	0.532 ± 0.048
1.626	1.552	1.697	−0.069 ± 0.027	0.617 ± 0.044
1.765	1.697	1.830	−0.176 ± 0.048	0.617 ± 0.079
		3 GeV/c		
0.097	0.082	0.114	0.272 ± 0.045	0.309 ± 0.064
0.131	0.114	0.150	0.291 ± 0.014	0.219 ± 0.020
0.170	0.150	0.192	0.286 ± 0.011	0.225 ± 0.019
0.214	0.192	0.238	0.302 ± 0.011	0.255 ± 0.016
0.262	0.238	0.288	0.309 ± 0.012	0.255 ± 0.017
0.314	0.288	0.342	0.303 ± 0.012	0.269 ± 0.017
0.370	0.342	0.400	0.306 ± 0.013	0.275 ± 0.016
0.430	0.400	0.461	0.286 ± 0.014	0.247 ± 0.019
0.493	0.461	0.526	0.297 ± 0.020	0.283 ± 0.028
0.559	0.526	0.593	0.227 ± 0.020	0.236 ± 0.029
0.628	0.593	0.663	0.246 ± 0.018	0.267 ± 0.026
0.736	0.663	0.810	0.218 ± 0.019	0.267 ± 0.026
0.926	0.810	1.044	0.168 ± 0.020	0.225 ± 0.029
1.165	1.044	1.288	0.183 ± 0.023	0.261 ± 0.033
1.411	1.288	1.534	0.206 ± 0.028	0.366 ± 0.039
1.658	1.534	1.780	0.124 ± 0.026	0.445 ± 0.037
1.900	1.780	2.019	0.090 ± 0.024	0.513 ± 0.034
2.135	2.019	2.249	0.010 ± 0.025	0.492 ± 0.035
2.396	2.249	2.538	−0.040 ± 0.026	0.519 ± 0.037
2.674	2.538	2.803	−0.162 ± 0.076	0.614 ± 0.107
		4 GeV/c		
0.120	0.097	0.145	0.190 ± 0.014	0.117 ± 0.020
0.172	0.145	0.201	0.213 ± 0.008	0.105 ± 0.011
0.232	0.201	0.265	0.222 ± 0.008	0.141 ± 0.013
0.300	0.265	0.337	0.226 ± 0.010	0.142 ± 0.013
0.376	0.337	0.417	0.207 ± 0.012	0.140 ± 0.016
0.459	0.417	0.503	0.197 ± 0.016	0.166 ± 0.024
0.549	0.503	0.596	0.170 ± 0.020	0.124 ± 0.030
0.645	0.596	0.695	0.173 ± 0.025	0.141 ± 0.036
0.746	0.695	0.798	0.146 ± 0.028	0.173 ± 0.041
0.963	0.798	1.136	0.132 ± 0.023	0.176 ± 0.033
1.316	1.136	1.500	0.145 ± 0.045	0.270 ± 0.063
1.688	1.500	1.878	0.181 ± 0.059	0.219 ± 0.085
2.069	1.878	2.258	0.246 ± 0.053	0.257 ± 0.076
2.446	2.258	2.631	0.175 ± 0.054	0.265 ± 0.078
2.812	2.631	2.989	0.006 ± 0.072	0.202 ± 0.104

TABLE I. (*Continued*)

$\bar{t}$ [(GeV/c)^2]	t_{min} [(GeV/c)^2]	t_{max} [(GeV/c)^2]	P	C_{NN}
		6 GeV/c		
0.115	0.098	0.133	0.110 ± 0.039	0.047 ± 0.052
0.152	0.133	0.173	0.115 ± 0.020	0.039 ± 0.027
0.195	0.173	0.218	0.132 ± 0.009	0.059 ± 0.013
0.242	0.218	0.268	0.131 ± 0.010	0.068 ± 0.013
0.295	0.268	0.323	0.134 ± 0.009	0.065 ± 0.013
0.352	0.323	0.382	0.127 ± 0.011	0.061 ± 0.015
0.413	0.382	0.446	0.120 ± 0.013	0.078 ± 0.018
0.479	0.446	0.514	0.110 ± 0.014	0.085 ± 0.020
0.549	0.514	0.586	0.096 ± 0.019	0.099 ± 0.027
0.624	0.586	0.662	0.091 ± 0.017	0.046 ± 0.025
0.702	0.662	0.742	0.091 ± 0.026	0.087 ± 0.036
0.783	0.742	0.826	0.069 ± 0.027	0.131 ± 0.037
0.869	0.826	0.913	0.092 ± 0.029	0.115 ± 0.040
1.003	0.913	1.096	0.094 ± 0.035	0.113 ± 0.048
1.192	1.096	1.291	0.126 ± 0.050	−0.013 ± 0.070
1.443	1.291	1.600	0.222 ± 0.058	0.124 ± 0.082
1.762	1.600	1.926	0.197 ± 0.093	0.088 ± 0.132

tributions on either side of the central peak are matched by scaling down the noncoplanar distribution and then subtracted yielding the elastic plot. These then are the signals used in determining P and C_{NN}.

The errors associated with these elastic event counts are strictly statistical and included the errors from both coplanar and noncoplanar and the events under the peak and those on the tails which are used to determine the background scale factor. This procedure is done for all θ_s, for both ϕ_s regions (0°–5°, 5°–10°) and for all four beam and target spin combinations.

This technique of background subtraction has been compared with the use of dummy targets (targets that approximate the nonhydrogen background) and has been shown to yield essentially the same results.[4]

These elastic events are then normalized to the total beam trigger (B) for each of the four spin combinations separately. Corrections were made to these beam trigger rates for events lost due to read-in failure and events that could not be analyzed because of beam-track-analysis failure. The normalized event counts are then used in a χ^2-minimization program. The method used is the variable-metric method for minimization originally developed at ANL.[28] The χ^2 minimized was

$$\chi^2 = \sum_{i=1}^{4} \sum_{j=1}^{N} \left\{ \left[\frac{(I^{ij}_{\text{data}} - I^{ij}_{\text{calc}})^2}{(\Delta I^{ij})^2} \right] + \frac{(P^{i}_{B\,\text{data}} - P^{i}_{B\,\text{calc}})^2}{\Delta P_B^2} \right\},$$

where I^{ij}_{data} and ΔI^{ij} are the number of normalized events and its error for the jth θ_s bin and ith spin combination. I^{ij}_{calc} is

$$I^{ij}_{\text{calc}} = I^{j}_{0} \left[1 + (P^{i}_{B\text{calc}} + P^{i}_{T}) P^{j} + P^{i}_{B\text{calc}} P^{i}_{T} C^{j}_{NN} \right]$$

and $I^{j}_{0} = \sum_{i=1}^{4} I^{ij}_{\text{data}}/4$. P and C_{NN} are allowed to vary to minimize χ^2. P_B is also varied to minimize the χ^2 with an error of ±0.05. P_T is kept fixed since its error was considered better than P_B. P_T is corrected, however, for the average ϕ_s angle of the data analyzed. P_T is thus really $P_T \langle \cos\phi_s \rangle$.

The final results are shown in Fig. 6 (along with the results of earlier experiments[29–31]) and are tabulated in Table I. The errors shown are purely statistical and do not include possible systematic errors. As mentioned earlier, the systematic error in calculating t is estimated to be less than 4%, which is in agreement with the 2-, 3-, and 4-GeV/c polarization data crossing zero at the correct 90°/c.m. angle. Because of the troubles in background subtraction, we estimate that for $|t|$ less than 0.15 (GeV/c)^2 the subtraction error may be comparable to the statistical error, and thus the total error should be approximately double that indicated in Table I. The background error for $|t| > 0.15$ quickly diminishes and we estimate that it is only about 10% of the statistical error.

Finally, because of possible errors in the beam and target polarization, the values of polarization may be shifted by as much as 5% of the quoted values and C_{NN} by 10%.

Because of the spread of ϕ_s values present in the data, the C_{NN} value we calculate should more

properly be called an effective C_{NN} since it is really

$$\langle\cos^2\phi_s\rangle C_{NN} + \langle\sin^2\phi_s\rangle C_{SS},$$

where S is the spin direction transverse to the beam and in the plane of scattering. But since $|\phi_s| < 10°$ and $\langle\sin^2\phi_s\rangle \approx 0.007$, the maximum possible contribution is smaller than our experimental error and can be neglected.

We note that there exists a normalization discrepancy in the polarization data at 3 GeV/c as shown in Fig. 6, where the data without the use of a polarized target by Neal *et al.*[29] are also plotted for comparison.

IV. DISCUSSION OF RESULTS

To completely describe pp elastic scattering, one would have to determine five complex amplitudes as functions of both $\theta_{\text{c.m.}}$ and W, total center-of-mass energy (see Appendix). At a given energy and scattering angle, it would require at least nine experiments to determine the amplitudes up to an overall phase and possibly 11 to resolve discrete phase ambiguities. With the inclusion of experimental errors, more than 11 experiments may be needed to determine a unique set of amplitudes. At present, however, there are not enough experimental quantities at any energy and angle to determine the amplitudes. One can, however, with the aid of assumptions and models attempt to find the amplitudes in certain kinematic regions.

One such approach is a phase-shift analysis. At low total energy one need only use a few partial waves to fit the entire angular region. Below the inelastic threshold (one-pion production) one can also use simple unitarity as an added constraint. Above threshold one can use a modified form of unitarity with the help of some model for inelastic scattering.

A preliminary phase-shift analysis has been performed by N. Hoshizaki[32] and his colleagues at Kyoto University using the 2- and 3-GeV/c data presented here, plus all other available data at these energies (i.e., differential cross sections, total cross sections, Re/Im ratio of amplitudes at $t=0$, $\Delta\sigma_T$, D_{NN}, R, and A'). The absorption of the higher partial waves ($J \geq 4$) was treated as being due to single- and double-pion production using the one-pion-exchange model of Amaldi[33] *et al.* and the measured cross section for one- and two-pion production. The real phase shifts were calculated from the one-boson-exchange model of Sawada[34] *et al.* The other, lower partial waves were allowed to vary freely.

Hoshizaki's group started with two solutions they had previously found from an earlier analysis[10] at 2.14 and 2.99 GeV/c. These two were chosen from a set of many similar solutions obtained from different starting points in their search and represented, in a sense, the spread of possible solutions with similar values for their χ^2.

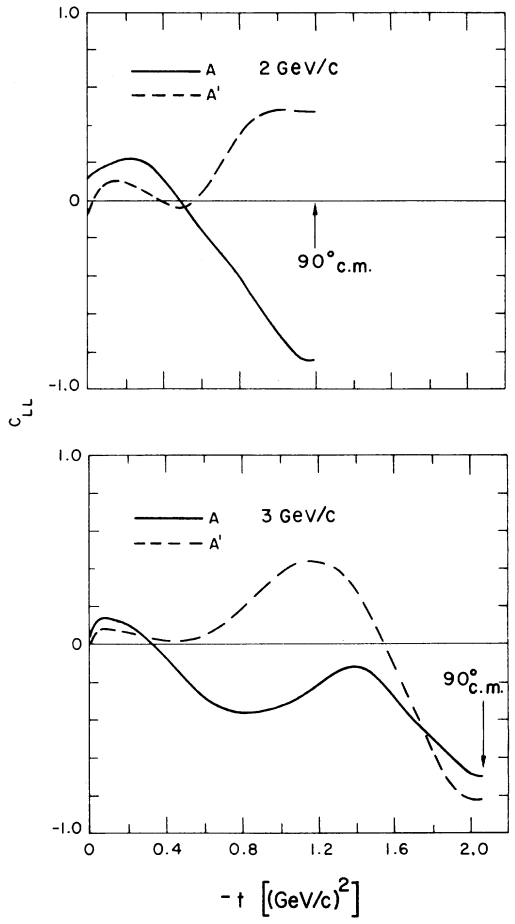

FIG. 7. Phase-shift predictions for C_{LL} at 2 and 3 GeV/c.

Using the present data and the two solutions, A and A', for the 2-GeV/c phase shifts, they obtained similar χ^2 values of about 55 for 72 data points and 17 adjustable parameters. At 3 GeV/c the χ^2 values were 106 and 79 for 90 data points and 17 adjustable parameters.

Since both solutions at 2 and 3 GeV/c give reasonably good χ^2 values, it appears, at least from this preliminary analysis, that the amplitudes have not yet been uniquely determined. In order to find which experiments would be useful to further reduce the range of acceptable solutions, one can made predictions of experimental results using these solutions and look for large discrepan-

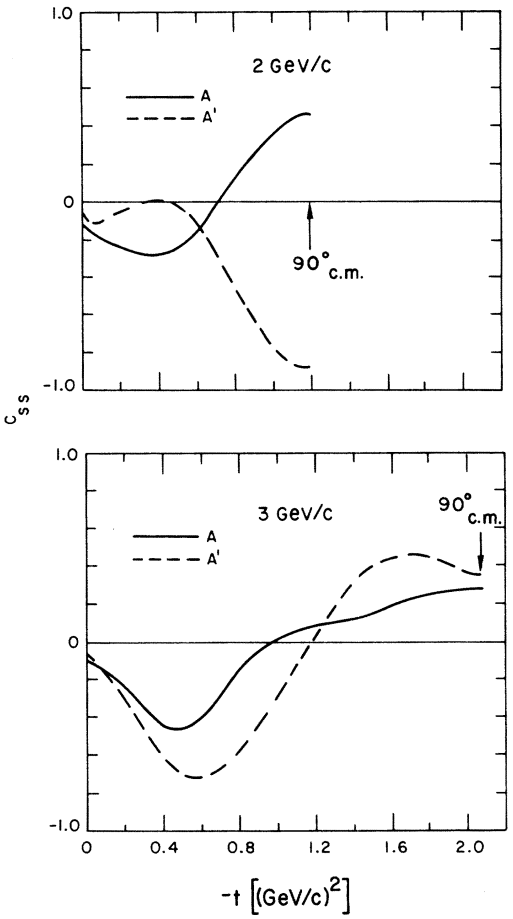

FIG. 8. Phase-shift predictions for C_{SS} at 2 and 3 GeV/c.

cies.

Among many possible candidates for experiments to perform are C_{LL}, C_{SS}, and $\Delta\sigma_L$. C_{LL} and C_{SS} are analogous to C_{NN} except with the initial spins polarized longitudinally and transversely, in the scattering plane, respectively. $\Delta\sigma_L$ is the difference in total cross section for initial spins antiparallel and parallel to $\Delta\sigma_L = \sigma(\rightleftarrows) - \sigma(\rightrightarrows)$. C_{LL} and C_{SS} predictions are shown in Figs. 7 and 8. Note that while there is some difference in predictions at low t, the largest differences occur around $|t| \approx 1.0$ (GeV/c)^2. The predictions for $\Delta\sigma_L$ at 2 GeV/c are -4.08 and 0.362 mb for solutions A and A'. At 3 GeV/c they are -1.27 and 1.88 mb. The value of $\Delta\sigma_L$ is particularly interesting since, combined with σ_{tot}, it yields the imaginary parts of ϕ_1 and ϕ_3 at $t=0$ (see Appendix). The C_{LL} and $\Delta\sigma_L$ experiments are currently being performed and the results will be presented in the near future.

At higher momenta (>3 GeV/c) phase-shift analyses become impractical to perform because of the large number of partial waves required and the presence of many more inelastic channels. Above 6 GeV/c several models[11-13] have been used to fit the available polarization and scattering data. One such fit by Field and Stevens[11] uses Regge amplitudes, plus corrections, to fit all previously available pp, $\bar{p}p$, and np elastic scattering and $\bar{p}p$ and np charge-exchange data. This parameterization included trajectories for P, f, ω, ρ, A_2, π, and B exchanges. In addition, lower-lying effective trajectories [$\alpha(0) = -0.5$ ($\tilde{f}$ and $\tilde{\omega}$)] were included to improve the fit for the lower energy data. From Fig. 6, one can see that the fit agrees with our polarization data quite well down to 3 GeV/c but has some trouble at 2 GeV/c. The comparison with C_{NN}, however, is not nearly as good. Within the present framework of their model, they cannot fit out data without adding one or more lower-lying trajectories [$\alpha(0) = -1, -1.5, \ldots$].

ACKNOWLEDGMENTS

We are indebted to R. Daly and W. Haberichter for their help with our multiwire proportional chamber system, to R. Miller for his assistance in computer-program development and polarized target preparation, and to Dr. S. T. Wang for assistance with the superconducting target magnet. We also wish to thank O. Fletcher, T. Kasprzyk, E. Millar, F. Onesto, and A. Rask for their help in setting up and running this experiment. We are grateful to Dr. A. Beretvas for helpful discussions.

APPENDIX

The helicity amplitudes are characterized by the helicities of the beam, target, scattered and recoil protons:

$$\phi = \langle \lambda_s, \lambda_R | \phi | \lambda_B, \lambda_T \rangle .$$

For protons λ can only have two values, $+1$ and -1, thus there are a total of 16 helicity amplitudes. However, due to parity, time reversal, and identical particles, there are only five independent amplitudes. These are[35,36]

$$\phi_1 = \langle ++ | \Phi | ++ \rangle ,$$

$$\phi_2 = \langle ++ | \Phi | -- \rangle ,$$

$$\phi_3 = \langle +- | \Phi | +- \rangle ,$$

$$\phi_4 = \langle +- | \Phi | -+ \rangle ,$$

$$\phi_5 = \langle ++ | \Phi | +- \rangle .$$

Some of the possible experimental observables, expressed in terms of helicity amplitudes, are as follows:

Observables $(B, T; S, R)$	Helicity amplitudes
$\sigma_0 = (0, 0; 0, 0)$	$\frac{1}{2}(\lvert\phi_1\rvert^2 + \lvert\phi_2\rvert^2 + \lvert\phi_3\rvert^2 + \lvert\phi_4\rvert^2 + \lvert 4\phi_5\rvert^2)$
$P = (0, N; 0, 0)$	$-\mathrm{Im}(\phi_1 + \phi_2 + \phi_3 - \phi_4)\phi_5^*/\sigma_0$
$= (N, 0; 0, 0)$	
$C_{NN} = (N, N; 0, 0)$	$\mathrm{Re}(\phi_1\phi_2^* - \phi_3\phi_4^* + 2\lvert\phi_5\rvert^2)/\sigma_0$
$D_{NN} = (0, N; 0, N)$	$\mathrm{Re}(\phi_1\phi_3^{\,2} - \phi_2\phi_4^{\,2} + 2\lvert\phi_5\rvert^2)/\sigma_0$
$C_{LL} = (L, L; 0, 0)$	$\mathrm{Re}(-\lvert\phi_1\rvert^2 - \lvert\phi_2\rvert^2 + \lvert\phi_3\rvert^2 + \lvert\phi_4\rvert^2)/(2\sigma_0)$
$C_{SS} = (S, S; 0, 0)$	$\mathrm{Re}(\phi_1\phi_2^* + \phi_3\phi_4^*)/\sigma_0$
$\sigma^{\mathrm{tot}} = (0, 0; 0, 0)$	$(2\pi/k)\mathrm{Im}(\phi_1 + \phi_3)_{t=0}$
$\Delta\sigma_T^{\mathrm{tot}} = (N, N; 0, 0)$	$-(4\pi/k)\mathrm{Im}(\phi_2)_{t=0}$
$\Delta\sigma_L^{\mathrm{tot}} = (L, L; 0, 0)$	$(4\pi/k)\mathrm{Im}(\phi_1 - \phi_3)_{t=0}$

The notation of the observables expresses the spin direction in the order of (beam, target; scattered, recoil).

†Work done under the auspices of the U. S. Energy Research and Development Administration.

[1]O. Benary, L. R. Price, and G. Alexander, UCRL Report No. 20000 NN, 1970 (unpublished).
[2]G. Cocconi, in *High Energy Collisions—1973*, proceedings of the Fifth International Conference, Stony Brook, edited by C. Quigg (AIP, New York, 1973).
[3]G. Barbiellini *et al.*, Phys. Lett. 39B, 663 (1972).
[4]G. Abshire *et al.*, Phys. Rev. Lett. 32, 1261 (1974).
[5]M. Borghini *et al.*, Phys. Lett. 24B, 77 (1967).
[6]M. Borghini *et al.*, Phys. Lett. 36B, 501 (1971).
[7]Proceedings of the Symposium on the High Energy Physics of Polarized Beams, edited by G. Thomas and A. Yokosawa, ANL Report No. ANL/HEP 7440 (unpublished).
[8]D. Miller *et al.*, Phys. Rev. Lett. 36, 763 (1976).
[9]M. H. Macgregor, M. J. Moravcsik, and H. P. Stapp, Annu. Rev. Nucl. Sci. 10, 291 (1960).
[10]N. Hoshizaki *et al.*, Prog. Theor. Phys. 42, 815 (1969); 42, 826 (1969); 45, 1123 (1971).
[11]R. D. Field and P. R. Stevens, ANL TAP Report No. ANL/HEP/CP-75-73 (unpublished).
[12]T.-Y. Cheng, S.-Y. Chu, and A. W. Hendry, Phys. Rev. D 7, 86 (1973).
[13]C. Bourrely, A. Martin, J. Soffer, and D. Wray, Report No. ANL/HEP-PR-75-41 (unpublished).
[14]M. Kac, Nucl. Phys. B62, 402 (1973).
[15]C. D. Jefferies, in *Proceedings of the Third International Symposium on Polarization Phenomena in Nuclear Reactions*, edited by H. H. Barschall and W. Haeberli (Univ. of Wisconsin Press, Madison, Wisconsin, 1971).
[16]W. deBoer, thesis, Report No. CERN 74-11, 1974 (unpublished).
[17]W. deBoer, J. Low Temp. Phys. 22, 85 (1976).
[18]J. J. Hill and D. A. Hill, Nucl. Instrum. Methods 116, 269 (1974).
[19]W. Haeberli, Annu. Rev. Nucl. Sci. 17, 373 (1967).
[20]A. Abragam and J. Winter, Phys. Rev. Lett. 1, 374 (1958).
[21]See reviews by L. G. Ratner and T. K. Khoe in Ref. 7.
[22]M. Froisart and R. Stora, Nucl. Instrum. Methods 7, 297 (1960).
[23]D. Cohen, Rev. Sci. Instrum. 33, 161 (1962).
[24]E. F. Parker *et al.*, IEEE Trans. Nucl. Sci. NS-22, 1718 (1975).
[25]J. B. Cladis, W. N. Ness, and B. J. Moyer, Phys. Rev. 87, 425 (1952).
[26]H. Tyren *et al.*, Nucl. Phys. 79, 321 (1966).
[27]Bruno Rossi, *High Energy Particles* (Prentice-Hall, Englewood Cliffs, New Jersey, 1952), Chap. 2, Sec. 16, p. 68, Eq. 9.
[28]W. C. Davidon, Report No. ANL-5990 (Rev. 2), 1966 (unpublished).
[29]H. Neal *et al.*, Phys. Rev. 161, 1374 (1967).
[30]M. Borghini *et al.*, Phys. Lett. 31B, 405 (1970).
[31]R. C. Fernow *et al.*, Phys. Lett. 52B, 243 (1974).
[32]Private communication.
[33]U. Amaldi *et al.* Nuovo Cimento 47, 85 (1967).
[34]S. Sawada *et al.*, Prog. Theor. Phys. 32, 380 (1964).
[35]C. Itzykson and M. Jacob, Nuovo Cimento 28, 1796 (1963).
[36]G. H. Thomas (see Ref. 7).